

# Stark tuning of telecom single-photon emitters based on a single $\text{Er}^{3+}$

Jian-Yin Huang,<sup>1,2</sup> Peng-Jun Liang,<sup>1,2</sup> Liang Zheng,<sup>1,2</sup> Pei-Yun Li,<sup>1,2</sup> You-Zhi Ma,<sup>1,2</sup> Duan-Chen Liu,<sup>1,2</sup> Jing-Hui Xie,<sup>1,2</sup> Zong-Quan Zhou,<sup>1,2,3,\*</sup> Chuan-Feng Li,<sup>1,2,3,†</sup> and Guang-Can Guo<sup>1,2,3</sup>

<sup>1</sup>CAS Key Laboratory of Quantum Information, University of Science and Technology of China, Hefei, 230026, China

<sup>2</sup>CAS Center for Excellence in Quantum Information and Quantum Physics,  
University of Science and Technology of China, Hefei, 230026, China

<sup>3</sup>Hefei National Laboratory, University of Science and Technology of China, Hefei 230088, China

(Dated: June 28, 2023)

The implementation of scalable quantum networks requires photons at the telecom band and long-lived spin coherence. The single  $\text{Er}^{3+}$  in solid-state hosts is an important candidate that fulfills these critical requirements simultaneously. However, to entangle distant  $\text{Er}^{3+}$  ions through photonic connections, the emission frequency of individual  $\text{Er}^{3+}$  in solid-state matrix must be the same, which is challenging because the emission frequency of  $\text{Er}^{3+}$  depends on its local environment. Herein, we propose and experimentally demonstrate the Stark tuning of the emission frequency of a single  $\text{Er}^{3+}$  in a  $\text{Y}_2\text{SiO}_5$  crystal by employing electrodes interfaced with a silicon photonic crystal cavity. We obtain a Stark shift of  $182.9 \pm 0.8$  MHz which is approximately 27 times of the optical emission linewidth, demonstrating the promising applications in tuning the emission frequency of independent  $\text{Er}^{3+}$  into the same spectral channels. Our results provide a useful solution for construction of scalable quantum networks based on single  $\text{Er}^{3+}$  and a universal tool for tuning emission of individual rare-earth ions.

PACS: 03.67.Hk, 42.50.-p

The photon loss is exponentially dependent on the length of fiber channels which prevent the long-distance transmission of quantum information. The quantum repeater approach has been proposed to solve this problem [1, 2] and has been implemented with various atomic systems [3–11]. These demonstrations are limited to a short distance due to the fact that the optical transitions of these atomic systems are far away from the telecom band. Although non-degenerate photon pairs [12–15] and quantum frequency conversion [16–18] have been employed in several works, they could introduce additional losses and noise.

Since  $\text{Er}^{3+}$  has natural optical transition in the telecom C band with long optical [19] and spin coherence lifetimes [20–22], it has been extensively studied in quantum networking applications, both as absorptive ensemble-based memories [23–29] and as emissive single-atom-based emitters [30–35]. By coupling with high- $Q$  micro/nano-photonic cavities, photoluminescence of  $\text{Er}^{3+}$  is enhanced in orders of magnitude and single  $\text{Er}^{3+}$  ions are able to be addressed optically [30, 35]. Spin manipulation and single-shot readout are subsequently demonstrated [31, 32], as well as controlling nearby nuclear spin as ancilla qubits [33]. Recently, the indistinguishability of successively emitted photons from a single  $\text{Er}^{3+}$  ion is verified with Hong-Ou-Mandel (HOM) interference [34]. For a single  $\text{Er}^{3+}$  quantum light source to be applicable in a realistic quantum repeater network, indistinguishability should be guaranteed for photons emitted from independent  $\text{Er}^{3+}$  ions as a prerequisite

to achieve entanglement swapping. However, because of complicated local environments inside a solid, different  $\text{Er}^{3+}$  dopants exhibit different optical transition frequencies. This could enable the spectral addressing of many independent ions [32], but the problem of wavelength alignments must be solved. For  $\text{Er}^{3+}$  ions coupled with nanophotonic cavities, the inhomogeneous broadening can typically reach several GHz, while the ions with sufficient Purcell enhancement are rare [30]. Therefore, a large-scale spectral tuning greater than 100 MHz is profitable to achieve indistinguishability. In this Letter, we propose and demonstrate Stark tuning of  $\text{Er}^{3+}$  in  $\text{Y}_2\text{SiO}_5$ , which has shown to be a simple and robust tool to tune spectra of single-atom based emitters.

$\text{Y}_2\text{SiO}_5$  is an often used host material due to its small magnetic moments ( $-0.137 \mu_N$  for  $^{89}\text{Y}$ ) and low natural abundance of magnetic isotopes (4.7% with  $-0.554 \mu_N$  for  $^{29}\text{Si}$ , 0.04% with  $-1.89 \mu_N$  for  $^{17}\text{O}$ ). In this work, the experiments were performed based on  $\text{Y}_2\text{SiO}_5$ , which have displayed good coherent properties for  $\text{Er}^{3+}$  [19–22]. The  $\text{Y}_2\text{SiO}_5$  crystal was grown by the Czochralski method in a 35-kW inductively heated generator at a 3-kHz middle frequency. The crystal is then cut along the optical extinction axes of  $D_1$ ,  $D_2$ , and  $b$  with dimensions of  $10 \times 8 \times 3 \text{ mm}^3$ . The purity of raw materials used for crystal growth is at least 99.999%. The concentration of  $\text{Er}^{3+}$  is less than 0.5 ppm as verified by the glow discharge mass spectrometry.

Single  $\text{Er}^{3+}$  ions need to be identified before studying the Stark effect. Since the optical excited state lifetime of  $\text{Er}^{3+}$  in bulk  $\text{Y}_2\text{SiO}_5$  is as long as 11 ms [36], the photon emission from a single  $\text{Er}^{3+}$  is too weak to be detected. Here, we follow the method of ref. [30] which adopted photonic crystal (PC) cavities to interface with

\* email: zq\_zhou@ustc.edu.cn

† email: cfli@ustc.edu.cn

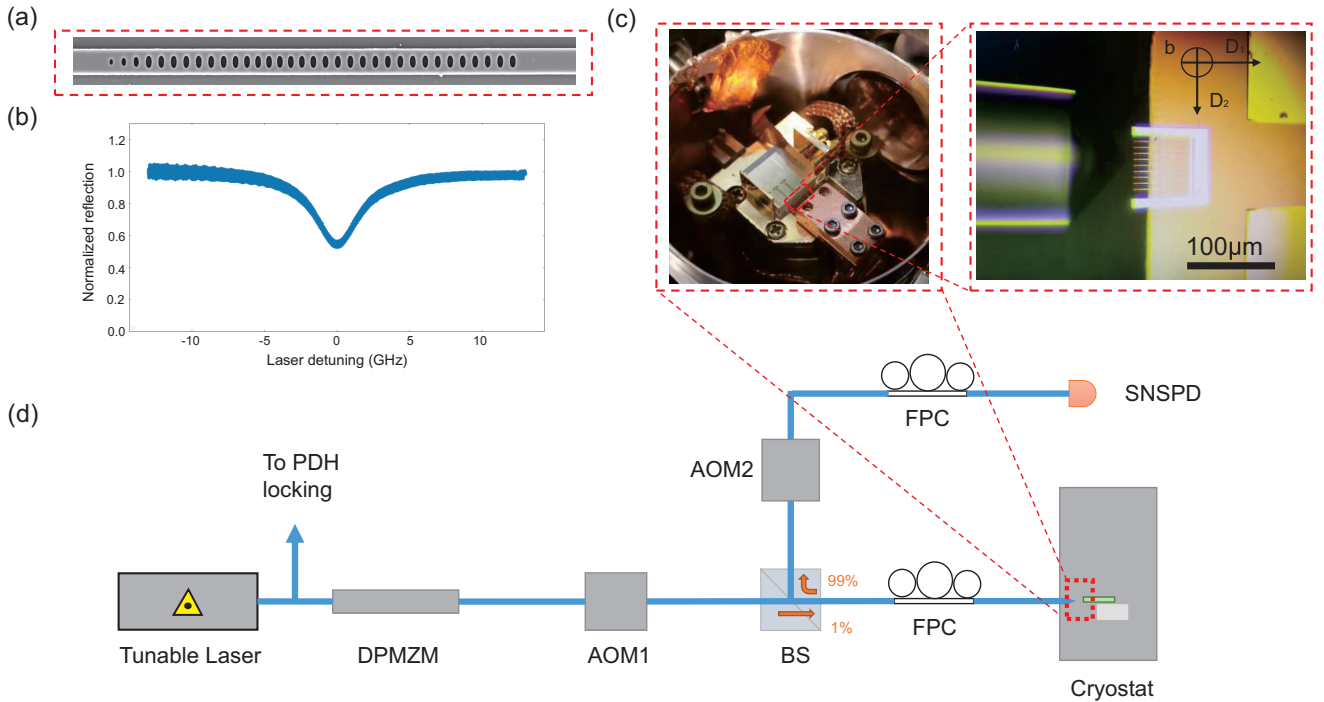


FIG. 1. (a) The scanning electron microscope image of the silicon photonic cavity structure before transferring to the surface of  $Y_2SiO_5$ . (b) Frequency reflection spectrum of the silicon photonic cavity used in these experiments, with a quality factor of  $5.1 \times 10^4$ . (c) Top-view image of the sample inside the cryostat. The photonic crystal cavity is placed on the  $D_1D_2$  plane of the  $Y_2SiO_5$  surface and in front of the electrode. The part that emerges from the edge of the sample is tapered waveguides, and they can be coupled to the lensed fiber with edge coupling. (d) Simplified diagram of the experimental setup. The laser frequency is stabilized to a high-finesse optical cavity. A dual-parallel Mach-Zehnder modulator (DPMZM) is employed for wideband sweeping of the excitation frequency during the acquisition of PLE spectra. The continuous laser is chopped by AOM1 into pulses to excite the ions. AOM2 is used to block the excitation light from entering the superconducting nanowire single-photon detector (SNSPD). The fiber polarization control (FPC) is used to control the laser polarization. The sample is situated in a 4 K cryostat.

$Er^{3+}$  ions for obtaining Purcell enhancement on the photon emission rate, and to improve the photon collection efficiency. The PC is fabricated on a silicon on insulator (SOI) wafer with a 220 nm device layer by electron beam lithography (EBL) and inductively coupled plasma (ICP), and then transferred onto the  $Y_2SiO_5$  crystal via the stamping technique [37]. A scanning electron microscope image (SEM) of the PC is presented in Fig. 1a. The quality factor of the PC cavity is approximately  $5.1 \times 10^4$  as measured with the cavity reflection spectrum (Fig. 1b). In order to achieve Stark tuning of the emission frequency, two additional electrodes are patterned on the host crystal's surface near the PC cavity to apply the required electric field on the target  $Er^{3+}$  ions. The electrode structure is fabricated with ultraviolet lithography, electron beam evaporation, and a lift-off process. The electrodes are 200  $\mu m$  wide and are 100  $\mu m$  apart from each other. The layout of the PC, the  $Y_2SiO_5$  crystal and the electrodes can be found in Fig. 1c. During the fabrication of the electrodes, the photoresist tends to be thicker at the crystal's edge compared to that at the center. Meanwhile, the  $Y_2SiO_5$  crystal is too thick and too brittle to allow chip-free splicing. For a lift-off pro-

cess with sufficient quality, two types of photoresists are spin-coated into two layers (LOR5A followed with S1813, both with 3000 rpm and 30 s), and a long exposure time of 51 s is adopted.

Fig. 1d presents the experimental configuration. A small portion of the laser (Toptica CTL 1500) is guided to a reference cavity to stabilize the laser frequency with the Pound–Drever–Hall (PDH) technique [38]. To scan the excitation frequency continuously, most laser power passes through a dual-parallel Mach-Zehnder modulator for single sideband frequency modulation. The laser pulses are chopped by using two consecutive double-passed acousto-optic modulators (AOMs), then enters the PC cavity via edge coupling to excite the ions. The fluorescence is gathered to the superconducting single-photon detector through the 99:1 beam splitter (BS) and two consecutive AOMs, which are used to prevent excitation pulses from influencing the detector. Two fiber polarization controllers (FPCs) are used to match the polarization to the PC cavity and to the detector. The single-photon detector has an 80% detection efficiency and 2 Hz dark counts. The overall photon collection efficiency is 1%, including excitation efficiency, transmission

efficiency, and detector efficiency.

We searched for single  $\text{Er}^{3+}$  by photoluminescence excitation (PLE) spectroscopy using resonant excitation. The excitation window and the detection window was separated in time. The PLE spectrum is given in Fig. 2. The series of sharp peaks are considered to result from photons emitted by individual  $\text{Er}^{3+}$  ions. Fig. 3a is a magnified image of the red-line area in Fig. 2. The peak marked with an asterisk is a representative single-ion PLE spectrum. The optical fluorescence lifetime of this ion was measured to be  $41.0 \pm 1.4 \mu\text{s}$ , as shown in Fig. 3b. This has been 278 times shorter compared with the bulk lifetime of 11.4 ms [36], showing the Purcell enhancement enabled by the atom-cavity interaction. The autocorrelation function  $g^{(2)}(0)$  [39] is measured to be  $0.10 \pm 0.04$  for this emission peak (Fig. 3c), confirming that this peak is indeed the signal from a single  $\text{Er}^{3+}$  ion. Here we denote this ion as “ion 1” for convenience in the following discussion. Although there are more peaks in the center of the inhomogeneous line, these peaks are typically overlaid with strong background noise coming from weakly-coupled ions, which would degrade the quality of output photons. Thus, all the ions in this study are searched on the tail of the inhomogeneous distribution.

The frequency shift of the atomic optical transition caused by a static electric field is well known as the DC Stark effect, which is the result of the differences in dipole moments and the polarizability between the excited and ground states. Usually, the induced frequency shift can be expressed as [40]:

$$h\Delta\nu = -\Delta\boldsymbol{\mu} \cdot \mathbf{L} \cdot \mathbf{E} - \frac{1}{2}\mathbf{E} \cdot \mathbf{L} \cdot \Delta\boldsymbol{\alpha} \cdot \mathbf{L} \cdot \mathbf{E} + \dots \quad (1)$$

where  $h$  is the Planck constant;  $\Delta\nu$  represents the optical frequency shift;  $\mathbf{L}$  is the local field correction tensor;  $\mathbf{E}$  is the electric field.  $\Delta\boldsymbol{\mu}$  and  $\Delta\boldsymbol{\alpha}$  are the differences between the ground and excited states in permanent dipole moment and polarizability, respectively. The omitted terms depend on the product of the local electric field with higher order hyperpolarization. The first-order linear Stark shift depends on the expectation values of the electric dipole moments for the optical ground and excited states. These values would vanish for the 1.5- $\mu\text{m}$  4f-4f transition of free  $\text{Er}^{3+}$  ions, or  $\text{Er}^{3+}$  ions occupying crystallographic sites with non-polar site symmetry. When doping into  $\text{Y}_2\text{SiO}_5$ , trivalent rare-earth ions such as  $\text{Er}^{3+}$  usually replace  $\text{Y}^{3+}$  which locate at sites with very low symmetry of  $C_1$ , and the linear Stark effect is maintained. In previous ensemble-based studies on rare-earth-doped  $\text{Y}_2\text{SiO}_5$  crystals, DC Stark shifts are dominated by the linear terms, and higher-order effects can be omitted [28, 29, 41, 42]. According to the measured data presented in Fig. 4, the Stark shifts of single  $\text{Er}^{3+}$  are also dominated by the linear terms, which are in consistency with the ensemble measurements, although much larger electric fields are applied compared with previous works.

In this work, the external electric field generated by the electrodes is aligned along the crystal’s  $D_2$  axis. A series of voltages are applied to the electrodes, and the frequency shifts of individual  $\text{Er}^{3+}$  ions are measured through PLE scanning. PLE spectra of ion 1 corresponding to different applied voltages are presented in Fig. 4a. It can be observed that the optical transition frequency shifts linearly along with the increased voltages. Since both  $\Delta\boldsymbol{\mu}$  and  $\mathbf{L}$  in Eq.(1) are anisotropic and unknown, here the linear Stark effect is described empirically as  $\Delta\nu = s_{\hat{n}}E_{\hat{n}}$ , where  $\hat{n}$  represents the unit vector along the  $D_2$  axis;  $E_{\hat{n}}$  is the electric field strength, and  $s_{\hat{n}}$  is the Stark coefficient. Due to technological limitations, the edge of the crystal is not suitable for gilding. As a result the PC is not in the center of the electrode, which can be seen in Fig. 1(c). Considering that the mode volume of the PC cavity is small, we approximate that the electric field at the center of the PC cavity is the electric field that the ion is experiencing. The values of  $E_{\hat{n}}$  are then extracted with numerical simulation based on the input voltages.  $s_{\hat{n}}$  of ion 1 is fitted as  $19.8 \pm 0.5 \text{ kHz}/(\text{V}\cdot\text{cm}^{-1})$ . The fitted line is given in Fig. 4b. Fig. 4a also reveals that the linewidth of the single  $\text{Er}^{3+}$  ion is slightly broadened as the voltage increases. This may be due to the fact that the increased voltage has made the  $\text{Er}^{3+}$  more sensitive to charge noise in its surroundings, which is similar to the phenomenon observed in color centers in diamonds [43, 44]. During the measurements the resonance frequency of the nanocavity experienced a persistent redshift of approximately 3 GHz/h, probably due to gas condensation [30]. To finish each PLE scanning in time, the corresponded frequency range of each curves in Fig. 4(a) is relatively narrow. Nevertheless, as shown in Fig. 3(a), the next peak in the redshift region is more than 300 MHz away from emission of ion 1, while the maximum tuning range for ion 1 is only 150 MHz. In addition, the frequency shift of these peaks has a linear dependence on the applied voltage. Therefore, these peaks displayed in Fig. 4(a) should all originate from ion 1. To recover the cavity resonance frequency for obtaining longer times for data acquisition, continuous laser light with a power greater than 100  $\mu\text{W}$  can be sent into the cryostat to sublimate the condensed gases on the nanocavity.

The Stark shifts of multiple individual  $\text{Er}^{3+}$  ions were further measured, and the results are presented in Fig. 4b. There appears to be two classes of ions experiencing red and blue shifts, respectively. Under an arbitrary external electric field, there can be up to four possibilities of Stark shifts for  $\text{Er}^{3+}:\text{Y}_2\text{SiO}_5$  because of the four orientations of a single crystallographic site [45]. Here  $\mathbf{E}$  is perpendicular to the b axis, and the four Stark shifts are pairwise degenerate. This leads to two types of Stark shifts with the same magnitude while in opposite directions. As shown in Fig. 4b, The Stark coefficients for different  $\text{Er}^{3+}$  ions are found to be diverse. For ions 1 to 6,  $|s_{\hat{n}}|$  has an average value of 20  $\text{kHz}/(\text{V}\cdot\text{cm}^{-1})$  and a standard deviation of 5.8  $\text{kHz}/(\text{V}\cdot\text{cm}^{-1})$ . The aver-

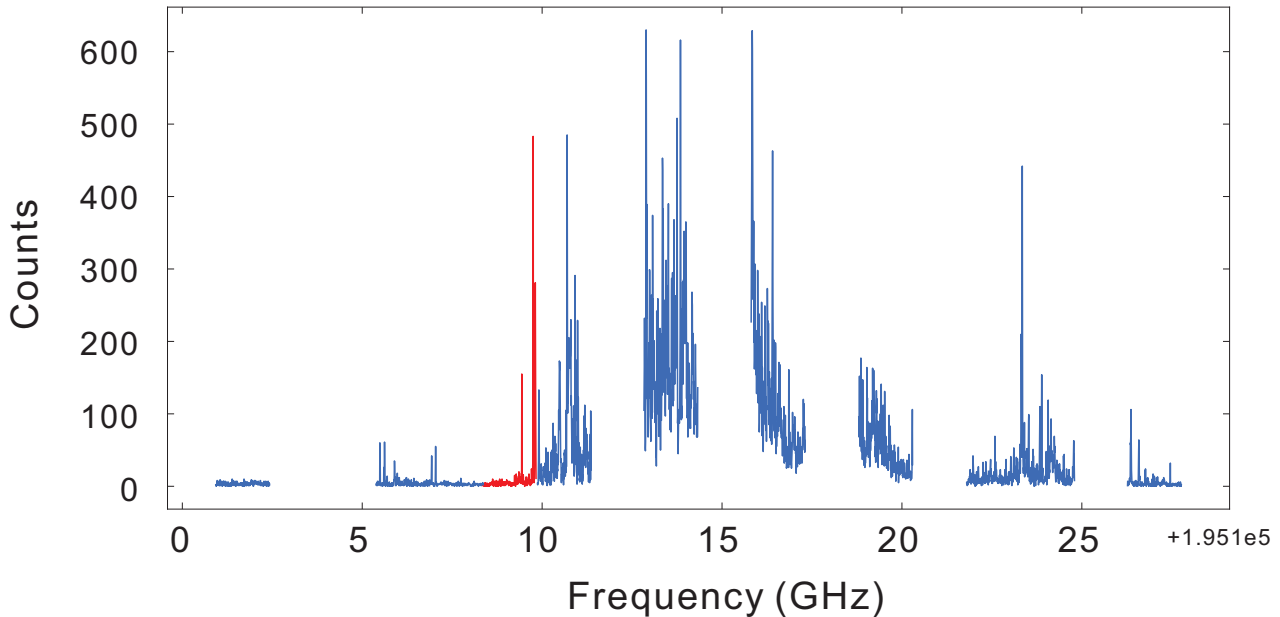


FIG. 2. PLE spectrum for normally undoped  $\text{Y}_2\text{SiO}_5$  crystal. The excitation frequency is swept around a center of 195115 GHz. The studied frequency range covers the absorption band of ensemble  $\text{Er}^{3+}$  in  $\text{Y}_2\text{SiO}_5$ . The intervals in the spectrum are caused by technical limitations in the vacuum degree of the current cryostat [30]. During the acquisition of the PLE spectrum, 10  $\mu\text{s}$  excitation pulses are repeated at a frequency of 10 kHz. Detection windows are arranged 1  $\mu\text{s}$  after the excitation pulses with a length of 85  $\mu\text{s}$ , during which AOM2 is turned on. The integration time is 5 s for each frequency point. The scan pitch is set as 5 MHz.

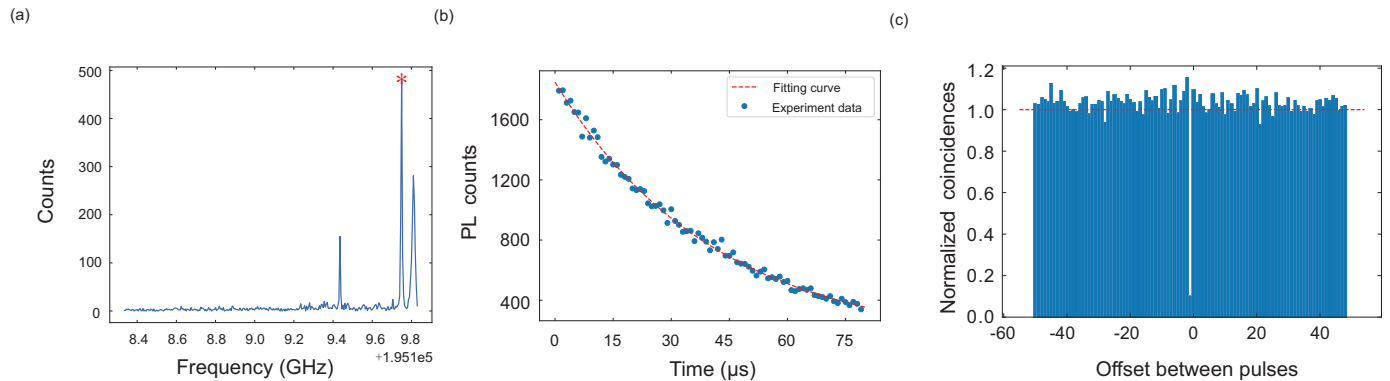


FIG. 3. (a) Magnified image of the red-line area in Fig. 2. (b) Fluorescence decay of a cavity-coupled single  $\text{Er}^{3+}$  ion. Experimental data are given in blue dots; the exponentially fitted curve is shown by a red dashed line. (c) Second-order autocorrelation function  $g^{(2)}$  measured for single  $\text{Er}^{3+}$  ion. The data in (b) and (c) were measured at the peak marked by asterisk in the PLE spectrum given in (a).

age value is consistent with the values reported in the ensemble-based experiment [46]. However, the deviation is unexpectedly large. In previous works [28, 29], which are also ensemble-based experiments working on the same material while  $\mathbf{E}$  is aligned parallel to the b axis, only slight antihole broadening is observed when DC voltage is applied. We speculate that this is because the  $\text{Er}^{3+}$  ions under study in this work are the ions with relatively

large Purcell effects. These ions are very close to the surface and their local environments are prone to be more complicated. We have also found one ion (ion 7) with an exceptionally deviated  $|s_{\hat{n}}|$  of  $9.8 \pm 0.3 \text{ kHz}/(\text{V}\cdot\text{cm}^{-1})$ , indicating that a significant defect may exist near this ion and such Stark-measurements could be a useful tool in probing local environments. Under the highest applied voltage of 333 V, the largest frequency shift of  $182.9 \pm$

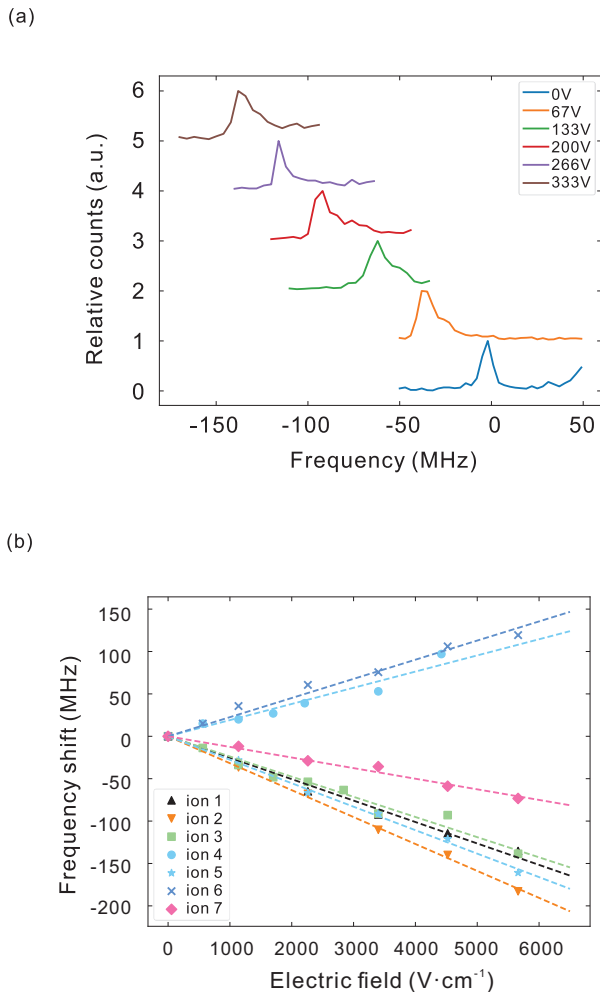


FIG. 4. (a) Frequency shifts of ion 1 as response to different voltages applied to the electrodes. (b) Stark shifts of multiple individual  $\text{Er}^{3+}$  ions. Measured data for each ion are linearly fitted.

0.8 MHz is achieved for ion 2, which is  $27.3 \pm 1.2$  times compared with its zero-field linewidth of  $6.7 \pm 0.3$  MHz.

In conclusion, we have performed a study on the Stark shift of single  $\text{Er}^{3+}$  ions in  $\text{Y}_2\text{SiO}_5$ . The Stark effect can be studied more directly and refined using the single-ion method compared with the ensemble method. In this work the maximum frequency shift reaches  $182.9 \pm 0.8$  MHz, which has been sufficient to tune two independent  $\text{Er}^{3+}$  ions into resonance. Greater frequency shifts can be achieved by further increasing the DC voltage or reducing the distance between the electrodes. For example, by further shrinking the electrode separation by 5 times and to mildly increase the applied voltages, Stark shift greater than 0.5 GHz can be expected. Meanwhile, the risk of possible dielectric breakdown caused by large electric field should be noticed and more tests should be performed. Our results demonstrate that Stark tuning is an efficient method for adjusting the emission wavelength of individual  $\text{Er}^{3+}$  ions, and it can be useful in future efforts to generate entanglement between two distant  $\text{Er}^{3+}$  ions in a quantum network.

J.-Y. H. and P.-J. L. contributed equally to this work.

*Note Added.* Recently, we became aware of independent work on the Stark tuning of single  $\text{Er}^{3+}$  emission in the  $\text{LiNbO}_3$  crystal by Yong Yu et al [47].

## ACKNOWLEDGMENTS

This work was supported by the National Key R&D Program of China (No. 2017YFA0304100), the Innovation Program for Quantum Science and Technology (No. 2021ZD0301200), the National Natural Science Foundation of China (Nos. 12222411 and 11821404) and this work was partially carried out at the USTC Center for Micro and Nanoscale Research and Fabrication. Z.-Q. Zhou acknowledges the support from the Youth Innovation Promotion Association CAS. The authors thank W. Liu, L. Chen, Y.-Z. He, and C. Tan for their assistance in micro and nano fabrication.

- 
- [1] H.-J. Briegel, W. Dür, J. I. Cirac, and P. Zoller, Quantum repeaters: the role of imperfect local operations in quantum communication, *Physical Review Letters* **81**, 5932 (1998).
- [2] N. Sangouard, C. Simon, H. De Riedmatten, and N. Gisin, Quantum repeaters based on atomic ensembles and linear optics, *Reviews of Modern Physics* **83**, 33 (2011).
- [3] H. Bernien, B. Hensen, W. Pfaff, G. Koolstra, M. S. Blok, L. Robledo, T. H. Taminiau, M. Markham, D. J. Twitchen, L. Childress, *et al.*, Heralded entanglement between solid-state qubits separated by three metres, *Nature* **497**, 86 (2013).
- [4] D. L. Moehring, P. Maunz, S. Olmschenk, K. C. Younge, D. N. Matsukevich, L.-M. Duan, and C. Monroe, Entanglement of single-atom quantum bits at a distance, *Nature* **449**, 68 (2007).
- [5] C.-W. Chou, J. Laurat, H. Deng, K. S. Choi, H. De Riedmatten, D. Felinto, and H. J. Kimble, Functional quantum nodes for entanglement distribution over scalable quantum networks, *Science* **316**, 1316 (2007).
- [6] X. Liu, J. Hu, Z.-F. Li, X. Li, P.-Y. Li, P.-J. Liang, Z.-Q. Zhou, C.-F. Li, and G.-C. Guo, Heralded entanglement distribution between two absorptive quantum memories, *Nature* **594**, 41 (2021).
- [7] B. Hensen, H. Bernien, A. E. Dréau, A. Reiserer, N. Kalb, M. S. Blok, J. Ruitenberg, R. F. Vermeulen, R. N. Schouten, C. Abellán, *et al.*, Loophole-free bell inequality violation using electron spins separated by 1.3 kilometres, *Nature* **526**, 682 (2015).

- [8] Y. Yu, F. Ma, X.-Y. Luo, B. Jing, P.-F. Sun, R.-Z. Fang, C.-W. Yang, H. Liu, M.-Y. Zheng, X.-P. Xie, *et al.*, Entanglement of two quantum memories via fibres over dozens of kilometres, *Nature* **578**, 240 (2020).
- [9] Z.-S. Yuan, Y.-A. Chen, B. Zhao, S. Chen, J. Schmiedmayer, and J.-W. Pan, Experimental demonstration of a BDCZ quantum repeater node, *Nature* **454**, 1098 (2008).
- [10] J. Hofmann, M. Krug, N. Ortegel, L. Gérard, M. Weber, W. Rosenfeld, and H. Weinfurter, Heralded entanglement between widely separated atoms, *Science* **337**, 72 (2012).
- [11] A. Delteil, Z. Sun, W.-b. Gao, E. Togan, S. Faelt, and A. Imamoglu, Generation of heralded entanglement between distant hole spins, *Nature Physics* **12**, 218 (2016).
- [12] C. Simon, H. De Riedmatten, M. Afzelius, N. Sangouard, H. Zbinden, and N. Gisin, Quantum repeaters with photon pair sources and multimode memories, *Physical Review Letters* **98**, 190503 (2007).
- [13] J. Fekete, D. Rieländer, M. Cristiani, and H. de Riedmatten, Ultranarrow-band photon-pair source compatible with solid state quantum memories and telecommunication networks, *Physical Review Letters* **110**, 220502 (2013).
- [14] D. Lago-Rivera, S. Grandi, J. V. Rakonjac, A. Seri, and H. de Riedmatten, Telecom-heralded entanglement between multimode solid-state quantum memories, *Nature* **594**, 37 (2021).
- [15] J. V. Rakonjac, D. Lago-Rivera, A. Seri, M. Mazzer, S. Grandi, and H. de Riedmatten, Entanglement between a telecom photon and an on-demand multimode solid-state quantum memory, *Physical Review Letters* **127**, 210502 (2021).
- [16] S. Zaske, A. Lenhard, C. A. Keßler, J. Kettler, C. Hepp, C. Arend, R. Albrecht, W.-M. Schulz, M. Jetter, P. Michler, *et al.*, Visible-to-telecom quantum frequency conversion of light from a single quantum emitter, *Physical Review Letters* **109**, 147404 (2012).
- [17] R. Ikuta, Y. Kusaka, T. Kitano, H. Kato, T. Yamamoto, M. Koashi, and N. Imoto, Wide-band quantum interface for visible-to-telecommunication wavelength conversion, *Nature Communications* **2**, 537 (2011).
- [18] A. Radnaev, Y. Dudin, R. Zhao, H. Jen, S. Jenkins, A. Kuzmich, and T. Kennedy, A quantum memory with telecom-wavelength conversion, *Nature Physics* **6**, 894 (2010).
- [19] T. Böttger, C. Thiel, R. Cone, and Y. Sun, Effects of magnetic field orientation on optical decoherence in  $\text{Er}^{3+}:\text{Y}_2\text{SiO}_5$ , *Physical Review B* **79**, 115104 (2009).
- [20] M. Rančić, M. P. Hedges, R. L. Ahlefeldt, and M. J. Sellars, Coherence time of over a second in a telecom-compatible quantum memory storage material, *Nature Physics* **14**, 50 (2018).
- [21] J.-Y. Huang, P.-Y. Li, Z.-Q. Zhou, C.-F. Li, and G.-C. Guo, Extending the spin coherence lifetimes of  $^{167}\text{Er}^{3+}:\text{Y}_2\text{SiO}_5$  at subkelvin temperatures, *Physical Review B* **105**, 245134 (2022).
- [22] J. V. Rakonjac, Y.-H. Chen, S. P. Horvath, and J. J. Longdell, Long spin coherence times in the ground state and in an optically excited state of  $^{167}\text{Er}^{3+}:\text{Y}_2\text{SiO}_5$  at zero magnetic field, *Physical Review B* **101**, 184430 (2020).
- [23] B. Lauritzen, J. Minář, H. De Riedmatten, M. Afzelius, N. Sangouard, C. Simon, and N. Gisin, Telecommunication-wavelength solid-state memory at the single photon level, *Physical Review Letters* **104**, 080502 (2010).
- [24] E. Saglamyurek, J. Jin, V. B. Verma, M. D. Shaw, F. Marsili, S. W. Nam, D. Oblak, and W. Tittel, Quantum storage of entangled telecom-wavelength photons in an erbium-doped optical fibre, *Nature Photonics* **9**, 83 (2015).
- [25] M. F. Askarani, T. Lutz, V. B. Verma, M. D. Shaw, S. W. Nam, N. Sinclair, D. Oblak, W. Tittel, *et al.*, Storage and reemission of heralded telecommunication-wavelength photons using a crystal waveguide, *Physical Review Applied* **11**, 054056 (2019).
- [26] I. Craiciu, M. Lei, J. Rochman, J. M. Kindem, J. G. Bartholomew, E. Miyazono, T. Zhong, N. Sinclair, and A. Faraon, Nanophotonic quantum storage at telecommunication wavelength, *Physical Review Applied* **12**, 024062 (2019).
- [27] J. S. Stuart, M. Hedges, R. Ahlefeldt, and M. Sellars, Initialization protocol for efficient quantum memories using resolved hyperfine structure, *Physical Review Research* **3**, L032054 (2021).
- [28] I. Craiciu, M. Lei, J. Rochman, J. G. Bartholomew, and A. Faraon, Multifunctional on-chip storage at telecommunication wavelength for quantum networks, *Optica* **8**, 114 (2021).
- [29] D.-C. Liu, P.-Y. Li, T.-X. Zhu, L. Zheng, J.-Y. Huang, Z.-Q. Zhou, C.-F. Li, and G.-C. Guo, On-demand storage of photonic qubits at telecom wavelengths, *Physical Review Letters* **129**, 210501 (2022).
- [30] A. Dibos, M. Raha, C. Phenicie, and J. D. Thompson, Atomic source of single photons in the telecom band, *Physical Review Letters* **120**, 243601 (2018).
- [31] M. Raha, S. Chen, C. M. Phenicie, S. Ourari, A. M. Dibos, and J. D. Thompson, Optical quantum nondemolition measurement of a single rare earth ion qubit, *Nature Communications* **11**, 1605 (2020).
- [32] S. Chen, M. Raha, C. M. Phenicie, S. Ourari, and J. D. Thompson, Parallel single-shot measurement and coherent control of solid-state spins below the diffraction limit, *Science* **370**, 592 (2020).
- [33] M. T. Uysal, M. Raha, S. Chen, C. M. Phenicie, S. Ourari, M. Wang, C. G. Van de Walle, V. V. Dobrovitski, and J. D. Thompson, Coherent control of a nuclear spin via interactions with a rare-earth ion in the solid state, *PRX Quantum* **4**, 010323 (2023).
- [34] S. Ourari, Lukasz Dusanowski, S. P. Horvath, M. T. Uysal, C. M. Phenicie, P. Stevenson, M. Raha, S. Chen, R. J. Cava, N. P. de Leon, and J. D. Thompson, Indistinguishable telecom band photons from a single erbium ion in the solid state, arXiv:2301.03564 (2023).
- [35] A. Ulanowski, B. Merkel, and A. Reiserer, Spectral multiplexing of telecom emitters with stable transition frequency, *Science Advances* **8**, eabo4538 (2022).
- [36] T. Böttger, Y. Sun, C. Thiel, and R. Cone, Spectroscopy and dynamics of  $\text{Er}^{3+}:\text{Y}_2\text{SiO}_5$  at 1.5  $\mu\text{m}$ , *Physical Review B* **74**, 075107 (2006).
- [37] G.-H. Lee, C.-H. Lee, A. M. Van Der Zande, M. Han, X. Cui, G. Arefe, C. Nuckolls, T. F. Heinz, J. Hone, and P. Kim, Heterostructures based on inorganic and organic van der waals systems, *APL Materials* **2**, 092511 (2014).
- [38] E. D. Black, An introduction to Pound–Drever–Hall laser frequency stabilization, *American Journal of Physics* **69**, 79 (2001).
- [39] A. Reiserer and G. Rempe, Cavity-based quantum networks with single atoms and optical photons, *Reviews of*

- Modern Physics **87**, 1379 (2015).
- [40] R. M. Macfarlane, Optical stark spectroscopy of solids, *Journal of luminescence* **125**, 156 (2007).
- [41] S. P. Horvath, M. K. Alqedra, A. Kinos, A. Walther, J. M. Dahlström, S. Kröll, and L. Rippe, Noise-free on-demand atomic frequency comb quantum memory, *Physical Review Research* **3**, 023099 (2021).
- [42] C. Liu, T.-X. Zhu, M.-X. Su, Y.-Z. Ma, Z.-Q. Zhou, C.-F. Li, and G.-C. Guo, On-demand quantum storage of photonic qubits in an on-chip waveguide, *Physical Review Letters* **125**, 260504 (2020).
- [43] L. De Santis, M. E. Trusheim, K. C. Chen, and D. R. Englund, Investigation of the stark effect on a centrosymmetric quantum emitter in diamond, *Physical Review Letters* **127**, 147402 (2021).
- [44] P. Tamarat, T. Gaebel, J. Rabeau, M. Khan, A. Greentree, H. Wilson, L. Hollenberg, S. Praver, P. Hemmer, F. Jelezko, *et al.*, Stark shift control of single optical centers in diamond, *Physical Review Letters* **97**, 083002 (2006).
- [45] O. Guillot-Noël, P. Goldner, Y. Le Du, E. Baldit, P. Monnier, and K. Bencheikh, Hyperfine interaction of  $\text{Er}^{3+}$  ions in  $\text{Y}_2\text{SiO}_5$ : An electron paramagnetic resonance spectroscopy study, *Physical Review B* **74**, 214409 (2006).
- [46] J. Minář, B. Lauritzen, H. de Riedmatten, M. Afzelius, C. Simon, and N. Gisin, Electric control of collective atomic coherence in an erbium-doped solid, *New Journal of Physics* **11**, 113019 (2009).
- [47] Y. Yu, D. Oser, G. D. Prato, E. Urbinati, J. C. Ávila, Y. Zhang, P. Remy, S. Marzban, S. Gröblacher, and W. Tittel, Frequency tunable, cavity-enhanced single erbium quantum emitter in the telecom band (2023), arXiv:2304.14685 [quant-ph].